Hindawi Publishing Corporation
Advances in Condensed Matter Physics
Volume 2016, Article ID 1562596, 7 pages
http://dx.doi.org/10.1155/2016/1562596

Research Article

Electronic and Magnetic Properties Studies on Mn and Oxygen Vacancies Codoped Anatase TiO_2

Zhongpo Zhou,[1,2,3] Xinwei Yang,[4] Haiying Wang,[1,2] Zhaorui Zou,[1,2] and Jingjing Guo[1,2]

[1]*College of Physics and Material Science, Henan Normal University, Xinxiang 453007, China*
[2]*Henan Key Laboratory of Photovoltaic Materials, Xinxiang 453007, China*
[3]*Key Laboratory of Artificial Micro- and Nano-Structures of Ministry of Education and School of Physics and Technology, Wuhan University, Wuhan 430072, China*
[4]*College of Electronic and Electrical Engineering, Henan Normal University, Henan 453007, China*

Correspondence should be addressed to Zhongpo Zhou; paul@whu.edu.cn and Haiying Wang; wanghaiy@whu.edu.cn

Received 11 June 2016; Accepted 23 August 2016

Academic Editor: Jörg Fink

The electronic and magnetic properties of Mn and oxygen vacancies codoped anatase TiO_2 were investigated. The calculated results showed that the TiO_2 codoped with Mn and oxygen vacancies have a magnetic moment value of 3.415 μ_B per $Ti_{31}MnO_{63}$ supercell. Furthermore, $Ti_{31}MnO_{63}$ gets the lowest energy with a geometrical optimization where the Mn ions locate at the nearest-neighbor sites of the oxygen vacancy. And experimental results indicated the magnetism is associated with the defects of Mn ions and oxygen vacancies induced by the Mn doping, which is consistent with the calculation results.

1. Introduction

Diluted magnetic semiconductors (DMSs), which are desirable for spintronic applications, have been extensively investigated for their magnetic and transport properties. Oxygen vacancies (V_Os) are important intrinsic defect in TiO_2 which can be manipulated by oxygen gas pressure in the process of the fabrication, and they could alternate the materials' properties significantly [1–10]. The origin of the observed ferromagnetism has been considered to be related closely to the V_Os instead of the cation vacancies reported by Wang et al. [11]. The magnetization enlarges as V_O content increases in oxygen-deficient TiO_2 ($TiO_{2-\delta}$) films observed by Yoon et al. [8]. And the carrier is n-type and the resistivity increases upon cooling [12] according to the transport measurements. Several theoretical investigations employed by first principle have been reported, most of which focus on cation vacancy in TiO_2 bulk materials [13–28]. However, less attention has been drawn to the V_O doped anatase TiO_2 and V_O-Mn codoped anatase TiO_2 in those researches.

There are three questions that should be figured out: (1) what is the electronic orbital composition of a V_O-induced state in detail for anatase TiO_2? (2) What is the electronic orbital geometry for the V_O-Mn induced states in V_O-Mn codoped anatase TiO_2? (3) What is the most stable structure for V_O-Mn codoped anatase TiO_2? It is necessary to bring further insight into the origin of the ferromagnetism in the TiO_2 with the transition-metal doping, where the V_Os play an important role in promoting long-range ferromagnetic order [29]. In this paper, we investigated the electronic and magnetic properties of Mn and V_Os codoped anatase TiO_2 ($Ti_{31}MO_{63}$) using the first-principles method based on the density functional theory (DFT). The experimental results are consistent with that of the first principles calculations, and the magnetism is associated with the V_O defect electrons induced by the Mn doping. The connections between the doped Mn ions and V_Os are discussed to explain the ferromagnetism observed in these materials.

2. Experiments and Model Calculations

The undoped TiO_2 films were fabricated by sol-gel spin coating. Step one: Mn-doped TiO_2 sol-gel solution preparation. In this step, titanium isoproxide (99%), absolute ethanol and

hydrochloric acid were used as starting materials. Firstly, 10 mL titanium isoproxide was dissolved in 70 mL absolute ethanol solution. The mixture was stirred for 5 min. Then 2 mL of 2 mol/L hydrochloric acid was added to the mixture and was stirred for 5 min. And then 30 mL absolute ethanol solution and proper weight of $MnCl_2$ (to obtain a doping concentration of 1 mol%, 3 mol%, 5 mol%, 7 mol%, and 9 mol% resp.) were added to the mixture and then were stirred for 24 h. Subsequently, the solution was kept stirred for 2 h with a heating magnetic stirrer until the sol-gel formed. Step two: the preparation of the Mn-doped anatase TiO_2 films using a spin coating method. Firstly, the fluorine-doped tin oxide (FTO) substrates were cleaned in de-ion water and in absolute ethanol solution for 5 min with ultrasonic cleaner, respectively. Then, the anatase TiO_2 films were prepared using TiO_2 sol-gel by the spin coating method. The spin rate was 400 rpm for 10 s and then was extended to 3000 rpm for 25 s. This spin coating procedure was repeated for five times to get the ideal film thickness of 800 nm. After coating, these samples were treated at 450°C in atmosphere for 2 h and cooled down naturally. All the reagents of acetone, absolute ethanol, titanium isoproxide, manganese dichloride, and hydrochloric acid were of analytical grade without further purification. The surface morphologies of TiO_2 films were observed by the scanning electron microscopy (SEM, S-4800). X-ray photoelectron spectroscopy (XPS, VG Multilab 2000x) was utilized to qualify and the chemical compositions and identify electronic structures. The binding energy of the XPS spectra was calibrated with the reference to the C 1 s peak at 284.6 eV. The magnetic properties were investigated using a vibrating sample magnetometer (VSM) equipped in the physical property measurement system (PPMS-9, Quantum Design).

First-principles calculations based on spin-polarized density-functional theory and projector augmented wave (PAW) pseudopotential technique are performed as implemented within the Vienna Ab-Initio Simulation Package (VASP) [30, 31]. The generalized gradient approximation (GGA-PBE) for the wave functions is used with a cutoff of 400 eV to model the exchange and correlation functional [32]. The calculations have been carried out for two cases: (1) an oxygen atom is substituted by a V_O; (2) a titanium (Ti) atom and an oxygen atom are substituted by a Mn atom and a V_O. The Monkhorst-Pack scheme k-points grid sampling was set to be $2 \times 2 \times 5$ for the 95-atom anatase supercell, $Ti_{31}MnO_{63}$ (corresponding to doping content of Mn ~ 3.13%). The valence electrons configuration for the O, Ti, and Mn are $2s^2\ 2p^4$, $3s^2\ 3p^6\ 3d^2\ 4s^2$, and $3d^5\ 4s^2$, respectively. All the atomic positions are fully optimized until the atom forces drop below the value 0.02 eV/Å. The DFT method has been proven to be one of the most accurate methods for the computation of the electronic structure of solids [4–7].

3. Results and Discussions

3.1. Electronic Properties and Magnetism of a V_O Doped TiO_2. According to the crystal field theory, due to the hybridization of Ti–O, the Ti 3d orbits split into two parts, the t_{2g} (d_{xy}, d_{xz}, d_{yz}) and e_g (d_{z2}, $d_{x2\text{-}y2}$) states. Geometrically, t_{2g} orbitals have lobes pointing between oxygen atoms, while e_g orbitals point toward oxygen. The O 2p orbit split into p_π and p_s states. O 2p and the t_{2g} (d_{xz}, d_{yz}) of Ti 3d devoted to the valence band (p_π devote to the top of valance band), while the conduction band was contributed by the d_{xy} and e_g of Ti 3d (d_{xy} devotes to the bottom of conduction band) [33]. In the ionic limit, each Ti gives four electrons to two oxygen atoms, resulting in the nominal charges of Ti^{4+} and O^{2-} [12]. When the V_O is introduced into the lattice, each V_O is assumed to donate two electrons. For Figure 1(b) (I), the TDOS of V_O-doped anatase TiO_2, there is a spin-split lower around the Fermi level illustrating the existence of magnetism. Such a state is stabilized in the spin-polarized DFT calculation (with a lower free energy of 0.0042 eV than the result of non-spin-polarized DFT calculation). The calculated net magnetic moment is about 0.533 μ_B. Figure 1(a) (II, III, and IV) shows the orbital decomposed density of states for three Ti 3d electrons nearest to the V_O. Three Ti atoms are labeled as Ti-II, Ti-III, and Ti-IV, with Ti-III and Ti-IV being equivalent with respect to the vacancy. It can be seen from the figure that, for Ti-II atom, the exchange spin-splitting at the bottom of the conduction band is mainly derived from the one e_g orbital (d_{xy}) and two t_{2g} orbitals (d_{yz} and d_{x2}), while the exchange spin-splitting at the bottom of the conduction band is mainly derived from the one e_g orbital (d_{z2}) and two t_{2g} orbitals (d_{yz} and d_{x2}) for Ti-II and Ti-IV atom. The orbitals overlap between the three Ti atoms nearest to the V_O. The hybridization between these three Ti 3d electron states leads to the electrons of Ti 3d spin-polarized. The charge distribution is illustrated in Figure 1(b). It can be seen that the state spread over all three Ti atoms adjacent to the vacancy and the local orbitals are the mixture of e_g and t_{2g} The charge distribution is similar to the charge distribution of the hybrid state in [12]. In the calculations, the results are obtained in a $Ti_{32}O_{63}$ anatase supercell with lowest total free energy for different V_O sites. The two electrons donated by one V_O are shared by the three Ti ions with up-spin forming Ti^{3+} ion to get the lowest energy. It is guessed that the appearance of the net magnetic moment in anatase TiO_2 may come from the larger crystal lattice distortion compared to rutile TiO_2.

3.2. Electronic Properties and Magnetism of V_O-Mn Codoped TiO_2. Magnetic properties of $Ti_{31}MnO_{63}$ were investigated using the first-principles methods based on the DFT. The lowest energies are achieved after geometrical optimization of $Ti_{31}MnO_{63}$ for each V_O-Mn codoping models, where doped Mn ions are located at the nearest-neighbor site of V_O. The result is similar to that of the report done recently [34].

In order to understand the nature of ferromagnetism, the electronic properties and magnetism of V_O-Mn codoped TiO_2 are investigated in detail. The lowest energy is obtained in the spin-polarized DFT calculation. Figure 2 shows the spin-resolved total density of states for the $Ti_{31}MnO_{63}$. The calculations show ferromagnetism with clear majority-spin defect states localized in the band gap for V_O-Mn codoped TiO_2. The major magnetic moment originates from the d electron of Mn ions. For V_O-Mn codoped TiO_2, the valence electrons configuration of doped Mn atom is $3d^5$. And the

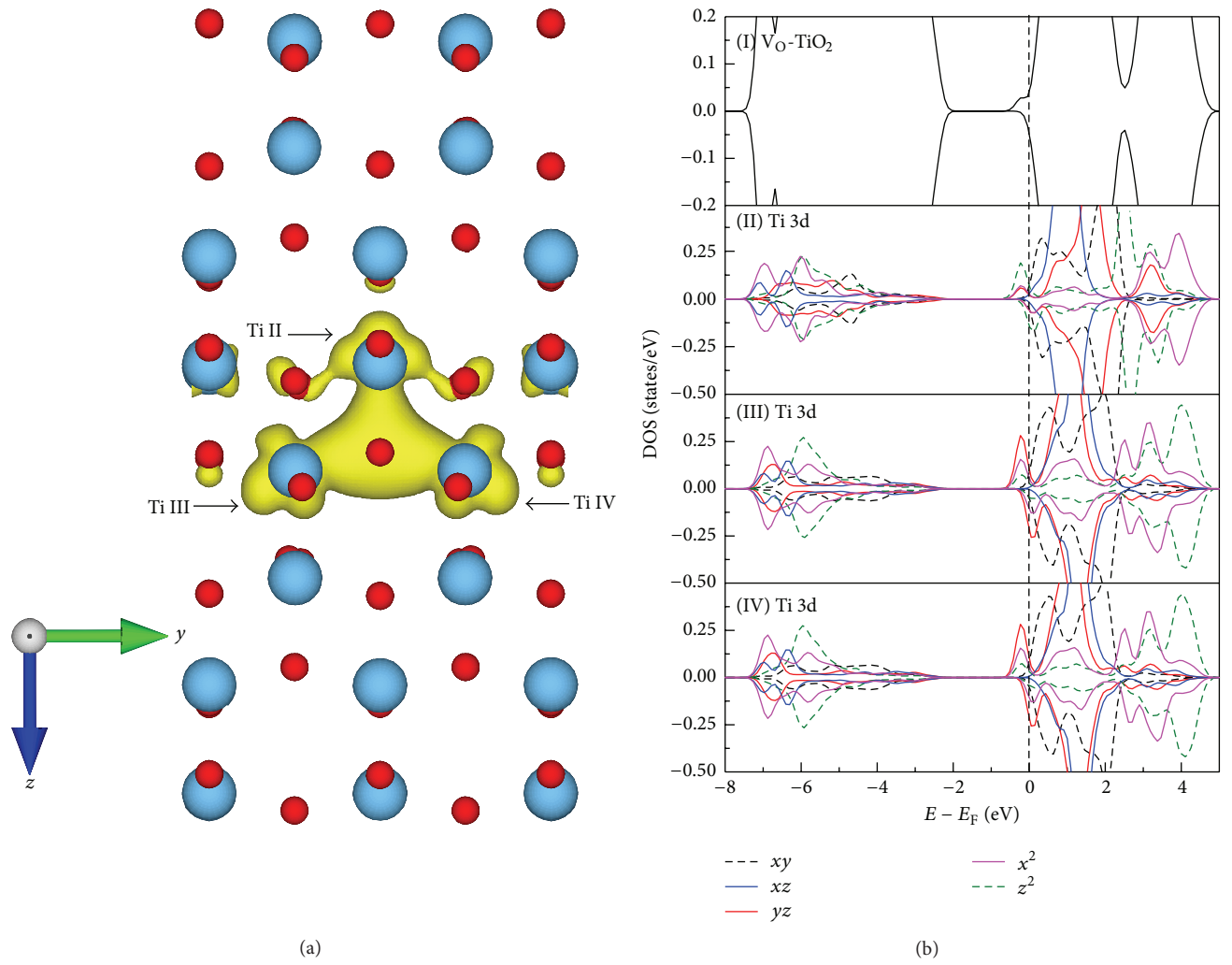

FIGURE 1: (a) Charge distribution of V_O-doped anatase TiO_2. (b) TDOS of V_O-TiO_2 and the orbitally decomposed density of states for three Ti 3d electrons nearest to V_O. The olive and black dashed curves represent the e_g bands; the red, blue, and magenta solid curves represent the t_{2g} bands, respectively.

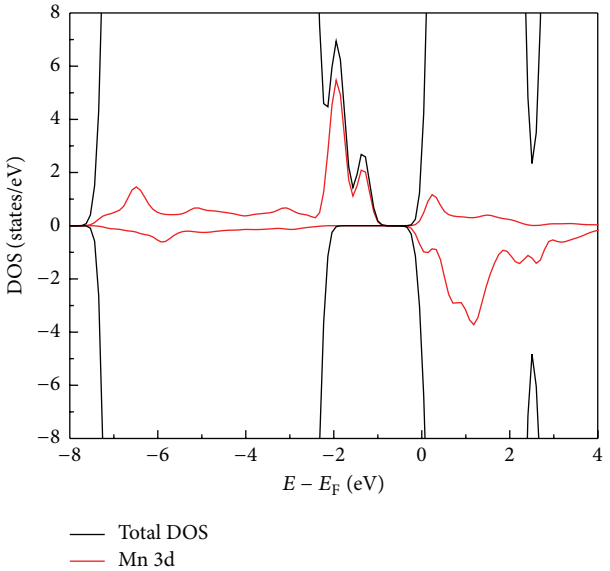

FIGURE 2: Spin-resolved total density of states for the Mn codoped TiO_2 in combination with an oxygen vacancy and spin- and orbital-resolved PDOS for the doped Mn atom.

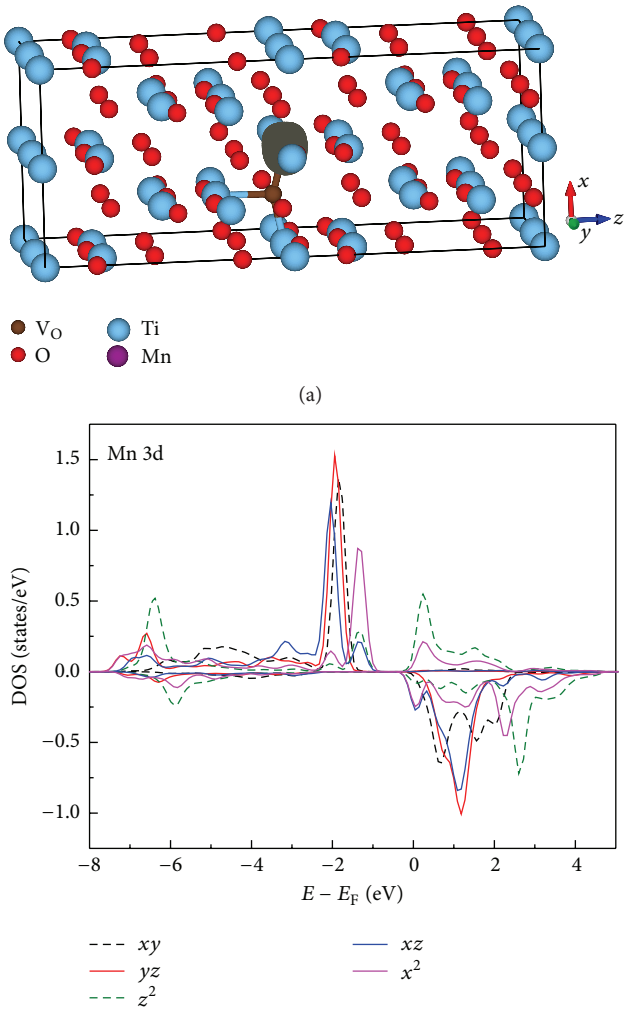

FIGURE 3: Isosurface plot of magnetization density (majority-spin minus minority-spin) for (a) $Ti_{31}MnO_{63}$ supercell; (b) the orbitally decomposed density of states projected on Mn ion.

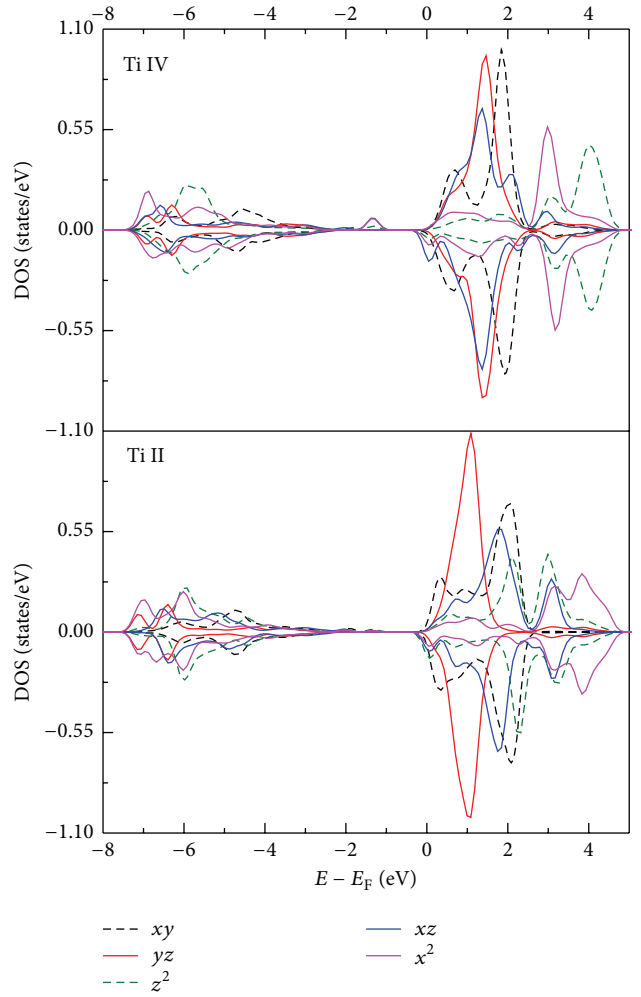

FIGURE 4: The orbital decomposed density of states projected on Ti II 3d electrons and Ti IV 3d electrons nearest to V_O for $Ti_{31}MnO_{63}$ supercell.

calculated net magnetic moment is about 3.415 μ_B, which is mainly contributed by doped Mn ion (calculated net magnetic moment is about 3.323 μ_B).

The isosurface plot of magnetization density (majority-spin minus minority-spin) for $Ti_{31}MnO_{63}$ supercell and the orbital decomposed density of states projected on Mn ion are shown in Figure 3. Spin density distribution of $Ti_{31}MnO_{63}$ supercell is shown in Figure 3(a). It can be noticed that the spin densities are mainly distributed on the doped Mn ion. It holds the spin with up direction. The values of calculated band lengths for V_O-Mn, V_O-Ti (III), and V_O-Ti (IV) are 1.8073 Å, 2.09822 Å, and 2.16686 Å, respectively. The lowest energy is achieved after geometrical optimization of $Ti_{31}MnO_{63}$, where one Mn ion is located at the nearest-neighbor site of V_O.

The orbital decomposed density of states projected on Mn ion is presented in Figure 3(b). There is a complete exchange spin-splitting of Mn 3d appearing within the Fermi level. The results indicate that there are t_{2g} and e_g states of Mn 3d electrons with up spin within the Fermi level. The valence electrons configuration on the Mn is $3s^2\ 3p^6\ 3d^5$. The orbital decomposed density of states projected on Ti II 3d electrons and Ti IV 3d electrons nearest to V_O for (a) $Ti_{31}MnO_{63}$ supercell is noticed in Figure 4. As it can be seen, there is almost no spin-splitting of Ti II 3d electrons and Ti IV 3d electrons nearest to V_O within the Fermi level. The results indicate that there are no electron states of Ti 3d electrons appearing within the Fermi level, which is consistent with the result of Figure 3. That just says that, due to the difference in the electronegativity and valence between Ti^{4+} ion and Mn^{2+} ions, the effect of the substitution is that no electron is donated to the TiO_2 lattice instead of two. Two electrons denoted by one V_O are captured by doped Mn ion and two electrons donated by the doped Mn^{2+} ion will be captured by five O ions nearest. As a result, the total net magnetic moment of V_O-Mn codoped TiO_2 is 3.415 μ_B.

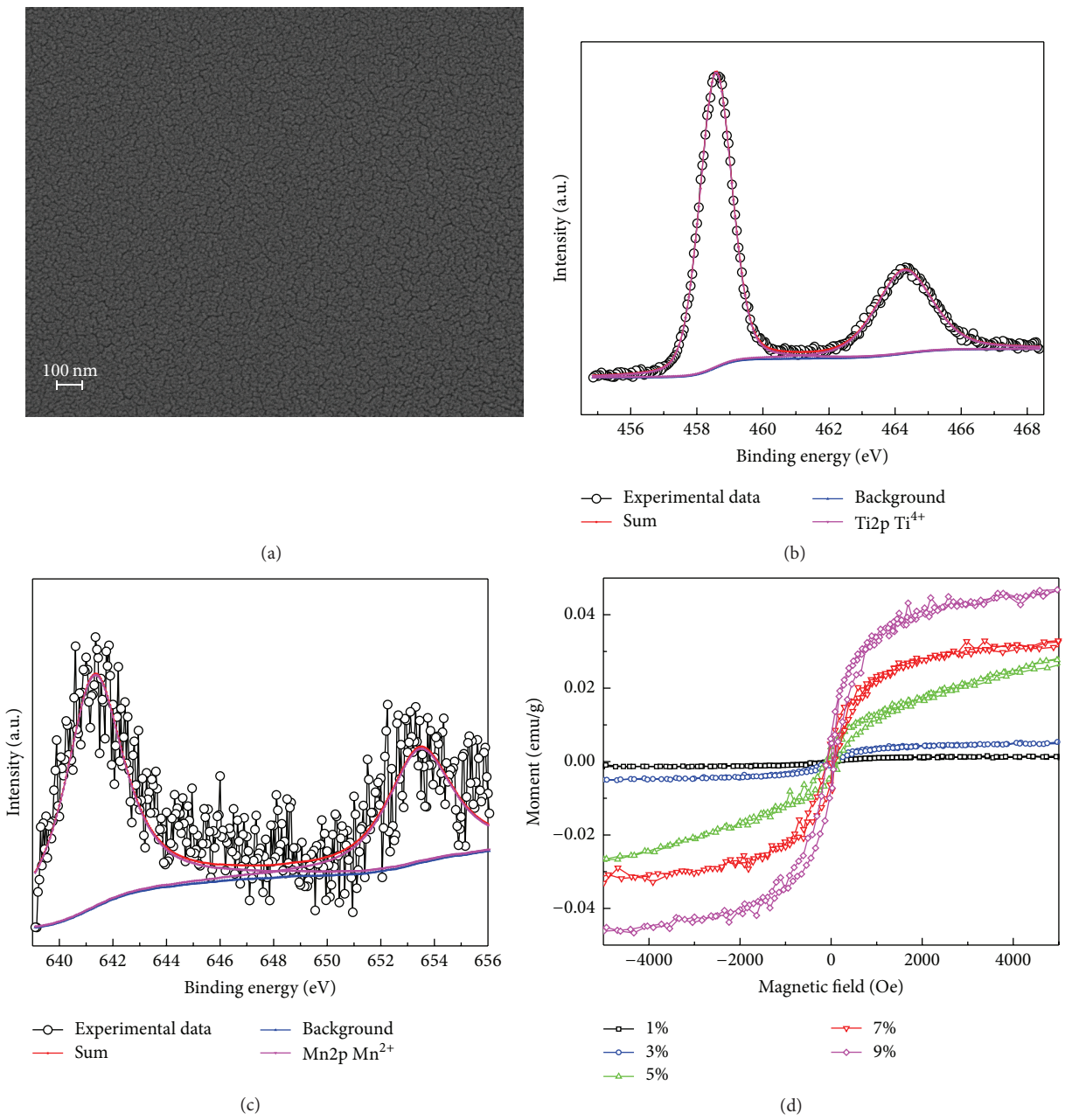

FIGURE 5: (a) SEM image of $Ti_{0.97}Mn_{0.03}O_2$ film; (b) XPS spectra of the core-level signal of Ti-2p and (c) Mn-2p of $Ti_{0.97}Mn_{0.03}O_2$ film; (d) magnetic hysteresis curves of the Mn-doped TiO_2 films with 1%, 3%, 5%, 7%, and 9% doping content measured at 300 K.

3.3. Experiment Results. The calculation results are confirmed by experimental data obtained for Mn-doped TiO_2 films. The Mn-doped TiO_2 films (with 1%, 3%, 5%, 7%, and 9% doping content) were grown by prepared by sol-gel spin coating. Figure 5(a) demonstrates the SEM images of the sample, which suggests that the film is smooth and the size of particles is about 10 nm.

The binding state of Ti and Co in the as-synthesized cobalt incorporated TiO_2 is analyzed with XPS. XPS analysis is performed after sputtering with Ar^+. The Ti-2p and Co-2p core levels spectra of the $Ti_{0.97}Mn_{0.03}O_2$ doped sample are shown in Figures 5(b) and 5(c). Figure 5(b) displays the Ti-2p core level XPS spectrum for $Ti_{0.97}Al_{0.03}O_2$ film sample. The open circles are the experimental data, the blue line is the background, the red line is the sum, and the peaks related to Ti^{4+} are fitted with magenta lines, where Ti 2p3/2 core level spectrum was fitted with combined Gaussian-Lorentzian functions. The main peak of Ti $2p^{3/2}$ situates around at 458.5 eV and a low intensity minor peak at 464.2 eV is attributed to Ti $2p^{1/2}$, close to the binding energies of the core-level of Ti^{4+} ion, which indicates the existence of Ti^{4+}. No signal of Ti^{3+} was detected. The Ti^{3+} ions were also not

observed in other Mn-doped films, which is not like the case of Nb- or Fe-doped TiO_2 films, due to the difference in the electronegativity and valence between Mn ion, Nb ion, and Fe ion [35, 36]. Figure 5(c) shows the Mn-2p core-level XPS spectrum for $Ti_{0.97}Mo_{0.03}O_2$ films. The open circles are the experimental data, the blue line is the background, the red line is the sum, and the peaks related to Mn^{2+} ion are fitted with magenta lines. The main peak of Mn $2p^{3/2}$ situates around at 641.2 eV and a low intensity minor peak at 653.6 eV is attributed to Mn $2p^{1/2}$, respectively, close to the binding energies of the core level of Mn^{2+} ion and lower to the binding energies of the core-levels of Mn^{3+} ion and Mn^{4+} ion, which indicates the existence of Mn^{2+}.

Figure 5(d) indicates the magnetic hysteresis (M-H) curves of Mn-doped samples (with 1%, 3%, 5%, 7%, and 9% doping content) at room temperature. All the Mn-doped samples showed ferromagnetism at room temperature (RT). The saturation magnetization M_S increases rapidly as the Mn content increases from 1% to 9%, alike other reports [37]. The magnetic moment per doped Mn atom exhibits more or less constant values for the 1% to 9% samples, up to the present experimental data.

Combining the calculation and experimental results presented above, we introduce a defect electron based model for the observed ferromagnetism. The magnetic moment associated with a $Mn^{2+}/V_O/Ti^{4+}$ complex is spread over two or more neighboring Ti sites. These moments are aligned ferromagnetic. The major contribution to the magnetic moment of our Mn-doped TiO_2 films comes from the unpaired d electron of Mn^{2+}, consistent with our first-principles calculation.

4. Conclusions

Electronic and magnetic properties of $Ti_{31}MnO_{63}$ have been studied combined with experiments and the first-principles calculations. Magnetic moment value is 3.415 μ_B per supercell for the V_O-Mn codoped anatase TiO_2. The lowest energy is achieved after geometrical optimization of $Ti_{31}MnO_{63}$, where doped Mn atoms are located at the nearest-neighbor site of V_O. Four electrons donated by the the V_O doped Mn^{2+} ion are shared by the nearest five O ions. The major magnetic moment originates from the d electron of Mn. Ferromagnetic behavior in V_O-Mn doped TiO_2 is corresponding to the strong Mn d-shell contribution and V_Os. The calculation results are confirmed by experimental data of Mn-doped TiO_2 films.

Competing Interests

The authors declare that there is no conflict of interests regarding the publication of this paper.

Acknowledgments

This work is supported by the NSFC nos. 11404100, 11175135, 10904116, and 11304083, the Post-Doctoral Research Foundation of Henan Province no. 01026500204, and the Scientific Research Foundation for PhD of Henan Normal University nos. 01026500257 and 01026500121. This work is also supported by the High Performance Computing Center of Henan Normal University.

References

[1] A. Fujishima and K. Honda, "Electrochemical photolysis of water at a semiconductor electrode," *Nature*, vol. 238, no. 5358, pp. 37–38, 1972.

[2] J. T. Yates Jr., "Photochemistry on TiO_2: mechanisms behind the surface chemistry," *Surface Science*, vol. 603, no. 10–12, pp. 1605–1612, 2009.

[3] B. Li, J. Zhao, K. Onda, K. D. Jordan, J. Yang, and H. Petek, "Ultrafast interfacial proton-coupled electron transfer," *Science*, vol. 311, no. 5766, pp. 1436–1440, 2006.

[4] M. Ramamoorthy, R. D. King-Smith, and D. Vanderbilt, "Defects on TiO_2 (110) surfaces," *Physical Review B*, vol. 49, no. 11, pp. 7709–7715, 1994.

[5] C. Di Valentin, G. Pacchioni, and A. Selloni, "Electronic structure of defect states in hydroxylated and reduced rutile TiO_2 (110) surfaces," *Physical Review Letters*, vol. 97, no. 16, Article ID 166803, 2006.

[6] U. Diebold, "The surface science of titanium dioxide," *Surface Science Reports*, vol. 48, no. 5–8, pp. 53–229, 2003.

[7] J. H. Lee and A. Selloni, "TiO_2 /ferroelectric heterostructures as dynamic polarization-promoted catalysts for photochemical and electrochemical oxidation of water," *Physical Review Letters*, vol. 112, no. 19, Article ID 196102, 2014.

[8] S. D. Yoon, Y. Chen, A. Yang et al., "Oxygen-defect-induced magnetism to 880 K in semiconducting anatase $TiO_{2-\delta}$ films," *Journal of Physics: Condensed Matter*, vol. 18, no. 27, pp. L355–L361, 2006.

[9] R. K. Singhal, S. Kumar, P. Kumari, Y. T. Xing, and E. Saitovitch, "Evidence of defect-induced ferromagnetism and its 'switch' action in pristine bulk TiO_2," *Applied Physics Letters*, vol. 98, no. 9, Article ID 092510, 2011.

[10] S. Zhou, E. Čižmár, K. Potzger et al., "Origin of magnetic moments in defective TiO_2 single crystals," *Physical Review B—Condensed Matter and Materials Physics*, vol. 79, no. 11, Article ID 113201, 2009.

[11] M. Wang, M. Feng, and X. Zuo, "First principles study of the electronic structure and magnetism of oxygen-deficient anatase TiO_2 (0 0 1) surface," *Applied Surface Science*, vol. 292, pp. 475–479, 2014.

[12] C. Lin, D. Shin, and A. A. Demkov, "Localized states induced by an oxygen vacancy in rutile TiO_2," *Journal of Applied Physics*, vol. 117, no. 22, Article ID 225703, 2015.

[13] Y. Bai and Q. Chen, "First principle study of the cation vacancy in anatase TiO_2," *Physica Status Solidi—Rapid Research Letters*, vol. 2, no. 1, pp. 25–27, 2008.

[14] H. Peng, J. Li, S.-S. Li, and J.-B. Xia, "Possible origin of ferromagnetism in undoped anatase TiO_2," *Physical Review B*, vol. 79, no. 9, Article ID 092411, 2009.

[15] J. Chen, L.-B. Lin, and F.-Q. Jing, "Theoretical study of F-type color center in rutile TiO_2," *Journal of Physics and Chemistry of Solids*, vol. 62, no. 7, pp. 1257–1262, 2001.

[16] B. J. Morgan and G. W. Watson, "A density functional theory + U study of oxygen vacancy formation at the (110), (100), (101), and (001) surfaces of rutile TiO_2," *The Journal of Physical Chemistry C*, vol. 113, no. 17, pp. 7322–7328, 2009.

[17] N. Yu and J. W. Halley, "Electronic structure of point defects in rutile TiO_2," *Physical Review B*, vol. 51, no. 8, pp. 4768–4776, 1995.

[18] E. Cho, S. Han, H.-S. Ahn, K.-R. Lee, S. K. Kim, and C. S. Hwang, "First-principles study of point defects in rutile TiO_{2-x}," *Physical Review B*, vol. 73, no. 19, Article ID 193202, 4 pages, 2006.

[19] M. M. Islam, T. Bredow, and A. Gerson, "Electronic properties of oxygen-deficient and aluminum-doped rutile TiO_2 from first principles," *Physical Review B*, vol. 76, no. 4, Article ID 045217, 2007.

[20] K. Yang, Y. Dai, B. Huang, and Y. P. Feng, "Density-functional characterization of antiferromagnetism in oxygen-deficient anatase and rutile TiO_2," *Physical Review B*, vol. 81, no. 3, Article ID 033202, 2010.

[21] A. Janotti, J. B. Varley, P. Rinke, N. Umezawa, G. Kresse, and C. G. Van de Walle, "Hybrid functional studies of the oxygen vacancy in TiO_2," *Physical Review B*, vol. 81, no. 8, Article ID 085212, 7 pages, 2010.

[22] S.-G. Park, B. Magyari-Köpe, and Y. Nishi, "Electronic correlation effects in reduced rutile TiO_2 within the LDA+U method," *Physical Review B*, vol. 82, no. 11, Article ID 115109, 2010.

[23] E. Finazzi, C. Di Valentin, G. Pacchioni, and A. Selloni, "Excess electron states in reduced bulk anatase TiO_2: comparison of standard GGA, GGA+U, and hybrid DFT calculations," *The Journal of Chemical Physics*, vol. 129, no. 15, Article ID 154113, 2008.

[24] G. Mattioli, P. Alippi, F. Filippone, R. Caminiti, and A. Amore Bonapasta, "Deep versus shallow behavior of intrinsic defects in rutile and anatase TiO_2 polymorphs," *Journal of Physical Chemistry C*, vol. 114, no. 49, pp. 21694–21704, 2010.

[25] A. Janotti, C. Franchini, J. B. Varley, G. Kresse, and C. G. Van de Walle, "Dual behavior of excess electrons in rutile TiO_2," *Physica Status Solidi—Rapid Research Letters*, vol. 7, no. 3, pp. 199–203, 2013.

[26] P. Deák, B. Aradi, and T. Frauenheim, "Quantitative theory of the oxygen vacancy and carrier self-trapping in bulk TiO_2," *Physical Review B*, vol. 86, no. 19, Article ID 195206, 2012.

[27] A. Malashevich, M. Jain, and S. G. Louie, "First-principles DFT + GW study of oxygen vacancies in rutile TiO_2," *Physical Review B*, vol. 89, no. 7, Article ID 075205, 2014.

[28] M. Setvin, C. Franchini, X. Hao et al., "Direct view at excess electrons in TiO_2 rutile and anatase," *Physical Review Letters*, vol. 113, no. 8, Article ID 086402, 2014.

[29] L. C. J. Pereira, M. R. Nunes, O. C. Monteiro, and A. J. Silvestre, "Magnetic properties of Co-doped TiO_2 anatase nanopowders," *Applied Physics Letters*, vol. 93, no. 22, Article ID 222502, 2008.

[30] G. Kresse and D. Joubert, "From ultrasoft pseudopotentials to the projector augmented-wave method," *Physical Review B*, vol. 59, no. 3, pp. 1758–1775, 1999.

[31] G. Kresse and J. Furthmüller, "Efficient iterative schemes for *ab initio* total-energy calculations using a plane-wave basis set," *Physical Review B*, vol. 54, no. 16, pp. 11169–11186, 1996.

[32] J. P. Perdew, K. Burke, and M. Ernzerhof, "Generalized gradient approximation made simple," *Physical Review Letters*, vol. 77, no. 18, pp. 3865–3868, 1996.

[33] Q. L. Chen, B. Li, G. Zheng, K. H. He, and A. S. Zheng, "First-principles calculations on electronic structures of Fe-vacancy-codoped TiO_2 anatase (101) surface," *Physica B*, vol. 406, no. 20, pp. 3841–3846, 2011.

[34] X. J. Wang, Y. L. Song, L. L. Tao et al., "Origin of ferromagnetism in aluminum-doped TiO_2 thin films: theory and experiments," *Applied Physics Letters*, vol. 105, no. 26, Article ID 262402, 2014.

[35] K. Bapna, R. J. Choudhary, S. K. Pandey, D. M. Phase, S. K. Sharma, and M. Knobel, "Electronic depiction of magnetic origin in undoped and Fe doped TiO_{2-d} epitaxial thin films," *Applied Physics Letters*, vol. 99, no. 11, Article ID 112502, 2011.

[36] J. Y. Yang, Y. L. Han, L. He, R. F. Dou, C. M. Xiong, and J. C. Nie, "d carrier induced intrinsic room temperature ferromagnetism in Nb:TiO_2 film," *Applied Physics Letters*, vol. 100, no. 20, Article ID 202409, 2012.

[37] A. Manivannan, M. S. Seehra, S. B. Majumder, and R. S. Katiyar, "Magnetism of Co-doped titania thin films prepared by spray pyrolysis," *Applied Physics Letters*, vol. 83, no. 1, pp. 111–113, 2003.